

Scattering using real-time path integrals

W. N. Polyzou

Department of Physics and Astronomy, The University of Iowa, Iowa City, IA 52242

Ekaterina Nathanson

School of Science and Technology, Georgia Gwinnett College, Lawrenceville, GA 30042

(Dated: November 30, 2017)

We investigate the possibility of using real-time path integrals to calculate scattering observables. The computational method is a numerical implementation of an interpretation of the path integral as the expectation value of a potential functional on a space of continuous paths with respect to a complex probability distribution. This investigation demonstrates the success of the method in a simple test model. How far it can be extended remains an open question.

PACS numbers:

I. INTRODUCTION

The purpose of this paper is to explore the possibility of using real-time path integral methods [1][2] to calculate scattering observables. The proposed computational method is based on a recent formulation of the path integral [3][4][5] that replaces the integral over paths by the expectation value of the potential functional, $F[\gamma] := e^{-i \int V(\gamma(t)) dt}$, with respect to a complex probability distribution on a space of paths. The space of paths is cylinder sets of continuous paths with fixed starting and end points.

The theory of complex probabilities was first contemplated by R. Henstock [6][7], based on a generalized theory of integration that he co-developed with J. Kurzweil. The Henstock-Kurzweil integral is similar to a Riemann integral, except the usual ϵ - δ definition is replaced by: for any prescribed error, ϵ , there is a positive function, $\delta(x)$ (called a gauge), where the intervals I_n and evaluation points x_n in the Riemann sums satisfy $I_n \in [x_n - \delta(x_n), x_n + \delta(x_n)]$. In the Henstock-Kurzweil case the points and intervals are correlated or tagged and the evaluation point is normally taken as one of the endpoints of the interval. Henstock-Kurzweil integral reduces to the Riemann when the gauge function, $\delta(x)$, is a constant.

One advantage is that the integral can still be approximated to arbitrary accuracy by generalized Riemann sums. The class of Henstock-integrable functions contains the Lebesgue measurable functions as well as functions that are not absolutely integrable. These considerations generalize infinite dimensionals integrals, which are inductive limits of finite dimensional integrals over cylinder sets that have a well-defined volume and correlated evaluation points and times. Precise definitions for the interested reader can be found in [3][4][5].

This motivated the replacement of a probability theory based on countably additive positive measures by one based on finitely additive generalized Riemann sums. The two formulations of probability coincide for real probabilities, but the Henstock formulation of probability extends to non-positive and complex probabilities. This was further developed by P. Muldowney. He developed a suggestion of Henstock that the Feynman path integral could be understood using this framework. Muldowney [3] proved that the method converges to a local solution of the Schrödinger equation. It was recently shown by P. Jørgensen and one of the authors [4][5] that the local solutions could be patched together to construct a global solution of the Schrödinger equation, and a unitary one-parameter time-evolution group. The time-evolution group is needed to formulate the scattering problem. In addition, the support of the complex probability is on paths that are almost everywhere continuous [5], leading to the interpretation of the path integral as the expectation of functionals of continuous paths with respect to a complex probability distribution.

The approach taken in this paper is a numerical implementation of the formulation based on computing the expectation of a potential functional with respect to a complex probability distribution. Gill and Zachary [8] investigated an alternative direct application of the Henstock integral to path integrals.

While this is just a reinterpretation of the ordinary path integral, it leads to a computational method that is not limited to quadratic potentials. In this paper this method is applied to treat a one-dimensional scattering problem with a Gaussian potential. While this is a simple problem, from a path integral perspective it involves computing a many-dimensional oscillating integral. The computational method used in this work computes the transition matrix elements in a straightforward, but inefficient way. While the efficiency of the method can be significantly improved, it remains to be seen whether the method can be scaled up to problems involving many particles or fields.

This purpose of this work is only to demonstrate that it is possible to perform scattering calculations using this method. An appealing property of the method is that the interpretation of the calculation as the expectation value of a potential functional with respect to a complex probability distribution on a space of paths is not lost in the

numerical implementation. In particular the computational algorithm can be deconstructed to find the approximate probability for any given cylinder set of paths.

Since the discussion that follows is somewhat detailed, a brief summary that outlines the essential elements of the computational method is given below. The new method starts like the ordinary path integral. It is based on the Trotter product formula [9], which is used to express the unitary time-evolution operator as a strong limit

$$e^{-iHt} = \lim_{N \rightarrow \infty} (e^{-i\frac{p^2}{2\mu} \frac{t}{N}} e^{-iV \frac{t}{N}})^N \quad (1)$$

provided that $\frac{p^2}{2\mu} + V$ is essentially self-adjoint. The next step is to insert complete sets of intermediate states that separately diagonalize both the kinetic energy, $p^2/2\mu$, and potential energy, V . The integrals over the intermediate momenta are Gaussian Fresnel integrals and can be performed analytically. What remains is the limit of N -dimensional integrals over the real line. Each integral is interpreted as an integral over all space at a given time slice. These steps are standard and can be found in any textbook that covers path integrals. The new steps are:

- 1 Replace each of the N integrals over the real line by a sum of integrals over small intervals. These intervals represent windows that a continuous path passes through at each time slice. The limit that the width of the finite intervals vanish, and the finite endpoints of the semi-infinite intervals become infinite is eventually taken. For computational purposes the intervals should be sufficiently small so that the potential is approximately constant on each interval and is approximately zero on the semi-infinite intervals.
- 2 The next step is to perform the integrals over the different products of N intervals, one for each time slice, *assuming that the potential is zero*. The results are complex quantities that are labeled by N intervals, $\{I_{n_1}, \dots, I_{n_N}\}$; one interval for each time slice. Each of sequence of intervals defines a cylinder set. A cylinder set is an ordered set of N windows at N intermediate times. Every continuous path goes through a unique cylinder set. It is elementary to show that the sum of these integrals over all possible N -fold products of intervals (cylinder sets) is 1. This allows them to be interpreted as complex probabilities that a path is an element of the associated cylinder set.
- 3 If the intervals are sufficiently small so the potential is approximately locally constant on each interval, then the sum of products of the complex probabilities with $e^{-i\sum V(x_i)\Delta t}$, where x_i is any sample point in the i^{th} interval in the cylinder set, converges to the “path integral” defined by the Trotter formula.

The new interpretation is that the ill-defined path integral is replaced by a well-defined expectation value of the potential functional with respect to a complex probability distribution on cylinder sets of continuous paths. This brief summary is discussed in more detail in what follows.

There are two problems that must be overcome to make this into a computational method. They can be summarized by noting that (1) it is not clear that the complex probabilities can be computed analytically; they involve N -dimensional integrals and (2) even if they could be computed either analytically or numerically, there are too many of them. If there are M intervals in each of N time slices, the number of cylinder sets is M^N , where the final result is obtained in the limit that both M and N become infinite.

The challenge of this work is to overcome these obstacles without giving up the interpretation of the path integral as the expectation value of a functional of paths with respect to a complex probability distribution of paths.

The virtue of this formulation of the “path integral” is that the non-existent path integral is replaced by the expectation value of a potential functional of continuous paths with respect to a complex probability distribution of cylinder sets of continuous paths.

While the test problem treated in this paper can be computed more efficiently by directly solving the Lippmann-Schwinger equation, path integrals are a powerful tool for solving problems in quantum field theory that are not limited by perturbation theory. While the methods discussed in this paper do not directly apply to the field theoretic case, they provide a different way of thinking about the problem that could lead to new computational strategies.

The paper is organized as follows. The next section includes a brief discussion of the scattering formalism that will be used in the rest of the paper. Section three discusses the conventional Feynman path integral formulation of the scattering problem. The fourth section introduces the reinterpretation of the path integral as the expectation value of the potential functional with respect to a complex probability on a space of continuous paths. Section five introduces a factorization of the complex probabilities that makes numerical computations possible. Section six analyzes the test calculation. A summary and concluding remarks appear in section seven.

II. SCATTERING OBSERVABLES USING TIME-DEPENDENT METHODS

The application that will be considered in this work is scattering in one-dimension using a Gaussian potential. The goal is to calculate sharp-momentum transition matrix elements using a path-integral treatment of time-dependent scattering. Because this method is ultimately based on the Trotter product formula, which requires a strong limit, the desired matrix elements need to be extracted using narrow wave packets.

In quantum mechanics the probability for scattering from an initial state $|\psi_i\rangle$ to a final state $|\psi_f\rangle$, is

$$P = |\langle\psi_f(t)|\psi_i(t)\rangle|^2 = |\langle\psi_f(0)|\psi_i(0)\rangle|^2. \quad (2)$$

The time-independence of the scattering probability follows from the unitarity of the time-evolution operator. Since this probability is independent of time, it can be computed at any convenient common time. In a scattering experiment the initial state, $|\psi_i(t)\rangle$, is simple long before the collision; it looks like a system of free moving particles, $|\psi_{i0}(t)\rangle$. Similarly, the final state, $|\psi_f(t)\rangle$, has a simple form long after the collision; it looks like a system of free moving particles, $|\psi_{f0}(t)\rangle$. The difficulty is that there is no common time when both states have a simple form. Time-dependent scattering theory provides a means to express the initial and final scattering states at a common time in terms of states of asymptotically free particles at a common time. The free particle states are easily computed at any time.

The relation of the initial and final states to the asymptotic system of free particles, described by $|\psi_{f0}(t)\rangle$ and $|\psi_{i0}(t)\rangle$, is given by the scattering asymptotic conditions

$$\lim_{t \rightarrow \infty} \||\psi_f(t)\rangle - |\psi_{f0}(t)\rangle\| = 0 \quad \lim_{t \rightarrow -\infty} \||\psi_i(t)\rangle - |\psi_{i0}(t)\rangle\| = 0 \quad (3)$$

which can be written as

$$\lim_{t \rightarrow \infty} \|e^{-iHt}|\psi_f(0)\rangle - e^{-iH_0t}|\psi_{f0}(t)\rangle\| = 0 \quad \lim_{t \rightarrow -\infty} \|e^{-iHt}|\psi_i(0)\rangle - e^{-iH_0t}|\psi_{i0}(t)\rangle\| = 0 \quad (4)$$

where $H = H_0 + V$ is the Hamiltonian of the system. The unitarity of the time-evolution operator, e^{-iHt} , leads to the equivalent forms:

$$\lim_{t \rightarrow \infty} \||\psi_f(0)\rangle - e^{iHt}e^{-iH_0t}|\psi_{f0}(0)\rangle\| = 0 \quad \lim_{t \rightarrow -\infty} \||\psi_i(0)\rangle - e^{iHt}e^{-iH_0t}|\psi_{i0}(0)\rangle\| = 0. \quad (5)$$

These formulas express the initial and final scattering states at the common time, $t = 0$, in terms of the corresponding non-interacting states at the same time.

While these expressions formally involve the limits $t \rightarrow \pm\infty$, if $t = 0$ is taken as the time of the collision, the limit is realized at the finite times when $\pm t$ are large enough for the interacting particles to be outside of the range of the interaction. In a real experiment the times when the beam and target are prepared and when the reaction products are seen in detectors are finite; the time limits are a simple way to ensure that t is large enough to reach the limiting form. This means that in a realistic calculation the limit can be replaced by a direct evaluation at a sufficiently large finite t or $-t$. The minimum size of this t depends on the range of the interaction, the size of the wave packets, and momentum distribution in the wave packet. When finite times are used in calculations, the minimal size of t needs to be determined for each problem.

Because it appears in equation (5) it is useful to define the operator

$$\Omega(t) := e^{iHt}e^{-iH_0t}. \quad (6)$$

The operator $\Omega(t)$ is a unitary operator that, for sufficiently large $\pm t$, transforms the initial or final *non-interacting* wave packet at time $t = 0$ to the initial or final interacting wave packet at $t = 0$. Equation (5) shows

$$|\psi_i(0)\rangle \approx \Omega(-t)|\psi_{i0}(0)\rangle \quad (7)$$

as t gets sufficiently large.

The primary quantities of interest are the on-shell transition matrix elements. For the simplest case of scattering by a short-range potential, $V(x)$, the transition matrix elements are related to $\Omega(t)$ by

$$\langle\mathbf{p}_f|T(E_i + i0^+)|\mathbf{p}_i\rangle = \lim_{t \rightarrow -\infty} \langle\mathbf{p}_f|V\Omega(t)|\mathbf{p}_i\rangle \quad (8)$$

where

$$T(z) = V + V(z - H)^{-1}V \quad (9)$$

is the transition operator and $E_i = \frac{\mathbf{p}_i^2}{2m} = \frac{\mathbf{p}_f^2}{2m}$. Because the limit on the right is a strong limit, it only exists if the sharp-momentum eigenstate, $|\mathbf{p}_i\rangle$, is replaced by normalizable a wave packet.

A useful approximation is to use a Gaussian wave packet, centered about the initial momentum, \mathbf{p}_i , with a delta-function normalization:

$$\int d\mathbf{p}\psi_{i0}(\mathbf{p}) = 1. \quad (10)$$

With this choice [10],

$$\langle \mathbf{p}_f | T(E_i) | \mathbf{p}_i \rangle \approx \langle \mathbf{p}_f | V\Omega(t) | \mathbf{p}_i \rangle \approx \langle \mathbf{p}_f | V\Omega(t) | \psi_{i0}(0) \rangle \quad (11)$$

in the large t , narrow wave packet limit. Gaussian wave packets are minimal uncertainty states, which provide maximal control over both the momentum resolution and spatial width of the wave packet. For computational purposes, the width of the wave packet should be chosen so $\langle \mathbf{p}_f | T(E_i) | \mathbf{p}_i \rangle$ varies slowly on the support of the wave packet.

In this work “path integral” methods are used to compute the right-hand side of equation (11). Because the path integral is formulated in terms of paths in the coordinate representation, the actual quantity that needs to be computed (in one dimension) is the Fourier transform

$$\langle p_f | V\Omega(t) | \psi_{i0}(0) \rangle = \frac{1}{\sqrt{2\pi}} \int dx e^{-ip_f x} \langle x | V\Omega(t) | \psi_{i0}(0) \rangle \quad (12)$$

for a sufficiently large t and narrow wave packet. This can be computed by a direct Fourier transform or by integrating over a narrow final-state wave packet, $\langle \psi_{f0}(0) |$, centered about p_f with a delta-function normalization:

$$\langle p_f | V\Omega(t) | \psi_{i0}(0) \rangle \approx \langle \psi_{f0}(0) | V\Omega(t) | \psi_{i0}(0) \rangle \quad (13)$$

III. SCATTERING USING THE FEYNMAN PATH INTEGRAL

The dynamical quantity needed as input to equation (11) is

$$\langle x | V\Omega(t) | \psi_{i0}(0) \rangle = \langle x | V e^{-iHt} | \psi_{i0}(-t) \rangle. \quad (14)$$

for sufficiently large t . The initial state at time zero is a Gaussian approximation to a delta function with the initial momentum, p_i :

$$\langle p | \psi_{i0}(0) \rangle = \frac{1}{2\sqrt{\pi}\Delta p} e^{-\frac{(p-p_i)^2}{4(\Delta p)^2}}. \quad (15)$$

Here Δp is the quantum mechanical uncertainty in p for this wave packet. This wave packet needs to be evolved to $-t$ using the free time evolution. The result is

$$\langle p | \psi_{i0}(-t) \rangle = \frac{1}{2\sqrt{\pi}\Delta p} e^{-\frac{(p-p_i)^2}{4(\Delta p)^2} + i\frac{p^2}{2\mu}t}. \quad (16)$$

These wave packets are needed in the coordinate basis in the path integral. The Fourier transform of (16) can be computed analytically

$$\langle x | \psi_{i0}(t) \rangle = (2\pi)^{-1/2} \sqrt{\frac{1}{1 + i\frac{2(\Delta p)^2 t}{\mu}}} e^{-\frac{(\Delta p)^2}{1 + \frac{4(\Delta p)^4 t^2}{\mu^2}} (x - \frac{p_i t}{\mu})^2} e^{i\frac{1}{1 + \frac{4(\Delta p)^4 t^2}{\mu^2}} (xp_i + 2x^2(\Delta p)^4 \frac{t}{\mu} - \frac{t}{\mu} \frac{p_i^2}{2})} = \quad (17)$$

$$(2\pi)^{-1/2} \sqrt{\frac{1}{1 + i\frac{t}{2(\Delta x)^2 \mu}}} e^{-\frac{1}{4\Delta x^2} \frac{1}{1 + \frac{i^2}{4\Delta x^4 \mu^2}} (x - \frac{p_i t}{\mu})^2} e^{i\frac{1}{1 + \frac{i^2}{4\Delta x^4 \mu^2}} (xp_i + \frac{x^2 t}{8\Delta x^4 \mu} - \frac{t}{\mu} \frac{p_i^2}{2})}. \quad (18)$$

where $\Delta p \Delta x = \frac{1}{2}$, since Gaussian wave functions represent minimal uncertainty states.

Equations (17) and (18) show that the center of this initial wave packet moves with its classical velocity, $v = p_i/\mu$, so the center of the wave packet is located at $x(t) = \frac{p_i t}{\mu}$, where μ is the mass and p_i is the mean momentum of

the initial wave packet. Ignoring the spreading of the wave packet, it will be in the range of the interaction for a time $t \approx \frac{R+\Delta x\mu}{|p_i|}$ where R is the range of the potential and Δx is the width of the wave packet. This suggests that the asymptotic time for scattering will be reached for $t > \frac{(R+\Delta x)\mu}{|p_i|}$. Because the potential appears in (11) in the expression for the transition matrix elements, only the values of $\langle x|e^{-iHt}|\psi_i(-t)\rangle$ inside the range of the potential are needed to calculate the transition matrix elements.

While the example of a single-particle interacting with a local potential in one dimension is used to test the proposed computational method, the computational method presented below formally generalizes to many-body reactions in three dimensions.

Equation (14) can be expressed exactly as

$$\langle x|Ve^{-iHt}|\psi_{i0}(-t)\rangle = \lim_{N \rightarrow \infty} \langle x_f|V \left(e^{-iHt/N} \right)^N |\psi_{i0}(-t)\rangle. \quad (19)$$

In the “ x ” representation equation (19) has the form

$$\int \langle x|e^{-i(\frac{p^2}{2\mu}+V)t}|x_i\rangle dx_i \langle x_i|\psi_{i0}(-t)\rangle = \lim_{N \rightarrow \infty} \int \langle x|(e^{-i(\frac{p^2}{2\mu}+V)\Delta t})^N|x_i\rangle dx_i \langle x_i|\psi_{i0}(-t)\rangle. \quad (20)$$

where $\Delta t := t/N$.

The only contributions to the large N limit come from the first-order terms in Δt . This follows from the Trotter product formula [9], which gives conditions for the operator version of

$$e^x = \lim_{N \rightarrow \infty} (1 + x/N)^N \quad (21)$$

to hold when $N \rightarrow \infty$ as a strong limit.

Using this property the limit in (20) can be replaced by

$$\lim_{N \rightarrow \infty} \langle x| \underbrace{e^{-i\frac{p^2}{2\mu}\Delta t} e^{-iV\Delta t} \dots e^{-i\frac{p^2}{2\mu}\Delta t} e^{-iV\Delta t}}_{N\text{-times}} |x_i\rangle dx_i \langle x_i|\psi_{i0}(-t)\rangle. \quad (22)$$

The following replacements were used in (20) to get (22)

$$e^{-i(\frac{p^2}{2\mu}+V)\Delta t} \rightarrow 1 - i\left(\frac{p^2}{2\mu} + V\right)\Delta t \rightarrow (1 - i\frac{p^2}{2\mu}\Delta t)(1 - iV\Delta t) \rightarrow e^{-i\frac{p^2}{2\mu}\Delta t} e^{-iV\Delta t}. \quad (23)$$

The next step is to insert complete sets of intermediate position and momentum eigenstates so $\frac{p^2}{2\mu}$ and V each become multiplication operators. This leads to the expression

$$\langle x_0|e^{-iHs}|\psi_{i0}(-t)\rangle = \lim_{N \rightarrow \infty} \int \prod_{n=1}^N \frac{dp_n dx_n}{2\pi} e^{ip_i(x_{n-1}-x_n) - i\frac{p_n^2}{2\mu}\Delta t - iV(x_n)\Delta t} \langle x_N|\psi_{i0}(-t)\rangle \quad (24)$$

where $x_0 = x$.

The p_n integrals are Gaussian Fresnel integrals and can be performed by completing the square in the exponent

$$\langle x_0|e^{-iHt}|\psi_{i0}(-t)\rangle = \lim_{N \rightarrow \infty} \int \prod_{n=1}^N \frac{dp_n dx_n}{2\pi} e^{-i\frac{\Delta t}{2\mu}(p_n - \frac{\mu}{\Delta t}(x_{n-1}-x_n))^2 + i\frac{\mu}{2\Delta t}(x_{n-1}-x_n)^2 - iV(x_n)\Delta t} \langle x_N|\psi_{i0}(-t)\rangle. \quad (25)$$

The general structure of the resulting momentum integrals is

$$\int_{-\infty}^{\infty} e^{-iap^2 + ibp} dp = \sqrt{\frac{\pi}{ia}} e^{ib^2/(4a)}. \quad (26)$$

These integrals are computed by completing the square in the exponent, shifting the origin, and evaluating the resulting integral by contour integration over a pie shaped path with one edge along the positive real p axis and the other making a 45 degree angle between the real and negative imaginary p axis.

The resulting integral over the N momentum variables is

$$\langle x_0|e^{-iHt}|\psi_{i0}(-t)\rangle =$$

$$\lim_{N \rightarrow \infty} \left(\frac{\mu}{2\pi i \Delta t} \right)^{N/2} \int \prod_{i=n}^N dx_n e^{i \frac{\mu}{2\Delta t} (x_{n-1} - x_n)^2 - iV(x_n) \Delta t} \langle x_N | \psi_{i0}(-t) \rangle. \quad (27)$$

This is the standard form of the path integral derived by Feynman. The path integral interpretation is obtained by factoring a Δt out of the sum to get

$$\langle x_0 | e^{-itH} | \psi_{i0}(-t) \rangle = \lim_{N \rightarrow \infty} \left(\frac{\mu}{2\pi i \Delta t} \right)^{N/2} \int e^{i \sum_{n=1}^N \left(\frac{\mu}{2} \left(\frac{x_{n-1} - x_n}{\Delta t} \right)^2 - V(x_n) \right) \Delta t} \prod_{m=1}^N dx_m \langle x_N | \psi_{i0}(-t) \rangle. \quad (28)$$

This looks like an integral over piece-wise linear paths between points in the N time slices, ($x_N \rightarrow x_{N-1} \rightarrow \dots \rightarrow x_0$), weighted with the imaginary exponential of a finite difference “approximation” of the action:

$$A \approx \sum_{n=1}^N \left(\frac{\mu}{2} \left(\frac{x_{n-1} - x_n}{\Delta t} \right)^2 - V(x_n) \right) \Delta t. \quad (29)$$

This is in quotes because, due to the integrals, the numerator in the finite difference does not get small as $\Delta t \rightarrow 0$, so the interpretation of $\frac{x_{i-1} - x_i}{\Delta t}$ as an approximate derivative is not justified.

Irrespective of any concerns about the interpretation, this expression is mathematically well-defined as a limit of finite dimensional integrals. It converges as a result of the Trotter product formula, however it is not very useful for computational purposes, except in the case of quadratic interactions, where the integrals can be computed analytically.

IV. THE MULDOWNNEY-NATHANSON-JØRGENSEN PATH INTEGRAL

To compute the path integral for scattering it is necessary to overcome several obstacles. These include the large dimensionality of the integrals, the need to compute with interactions that are more general than quadratic, the oscillatory nature of the integrals, and the spreading of the scattering wave packets. The purpose of this work is to investigate some methods that have the potential to overcome these obstacles.

The proposed computations are a consequence of the reformulation of the path integral due to Muldowney [3], Nathanson and Jørgensen [4][5]. This provides a means for treating a large class of interactions, and eliminates the questionable “finite difference” approximation of the kinetic energy in (28). There still remain oscillations associated with the potential term; but they are only relevant inside of the finite range of the potential.

This method replaces the usual interpretation of the path integral by assigning a “complex probability” to subsets of continuous paths, and computing the expectation value of the random variable $F[\gamma] = e^{-i \int V(\gamma(t)) dt}$ with respect to this complex probability distribution. In this expression $\gamma(t)$ is a continuous path between x_N and x_0 , This differs from the standard interpretation in that the action functional is replaced by a potential functional, and the “measure” is replaced by a complex probability distribution. The random variable $e^{-i \int V(\gamma(t)) dt}$ differs from 1 only on the portion of the path, $\gamma(t)$, that is in the range of the potential. The potential functional does not suffer from the interpretational difficulties of the action functional in the standard path integral.

This is still a computationally intractable problem. In order to make this computationally tractable, the complex probability is approximately factored into a product of complex probabilities for each “time step”. These one-step “complex probabilities” have the advantage that they can be computed analytically and that the analytic calculation treats the free propagation exactly. The important simplification is that the one-step complex probability can be approximated by a matrix and the multi-step probability is approximately the N -fold product of the same matrix. This reduces the calculation of the transition matrix elements to the computation of powers of a matrix. In this case the usual Monte Carlo integration is replaced by matrix multiplication, which can be performed efficiently even for large matrices.

Finally, the use of the operator $\Omega(t)$ in (6) means that the quantity being computed in (8) and (11) is a deformation of the initial free wave packet, at the time of collision, to the corresponding interacting packet at the same time. In this case both the free and interacting wave packets remain localized near the origin and the parameter t interpolates between the free and interacting localized states. The spreading of the wave packet is only relevant during the time of collision, and even during that time one expects some cancellations. Thus, the relevant parts of the calculation take place in a finite space-time volume.

The fundamental new idea that is the key to the computational strategy, proposed by Muldowney, is to decompose the integral over each x_n in (27) into a sum of integrals over $M_n + 1$ intervals, I_{mn} , at the n^{th} time slice:

$$\int dx_n = \sum_{m=0}^{M_n} \int_{I_{mn}} dx_n. \quad (30)$$

The intervals I_{mn} are chosen to be disjoint and cover the real line. They are taken to have the general form

$$\underbrace{(-\infty, x_{1n})}_{I_{0n}}, \underbrace{[x_{1n}, x_{2n})}_{I_{1n}}, \dots, \underbrace{[x_{M-1,n}, x_{M,n})}_{I_{M-1,n}}, \underbrace{[x_{M,n}, \infty)}_{I_{M,n}}. \quad (31)$$

Using this decomposition the limit in (28) becomes

$$\langle x_0 | e^{-itH} | \psi_{i0}(-t) \rangle = \lim_{N \rightarrow \infty} \left(\frac{\mu}{2\pi i \Delta t} \right)^{N/2} \sum_{m_1 \dots m_N} \prod_{n=1}^N \int_{I_{m_n}} dx_n e^{i \frac{\mu}{2\Delta t} (x_{n-1} - x_n)^2 - iV(x_n)\Delta t} \langle x_N | \psi_{i0}(-t) \rangle. \quad (32)$$

The sum is over the $(M_1 + 1) \times \dots \times (M_N + 1)$ N -fold Cartesian products of intervals (cylinder sets) for the N time slices. Each continuous path from x_N to x_0 goes through one interval in each time slice and is thus an element of a unique cylinder set. The m_n sums range over $0 \leq m_n \leq M_n$, $1 \leq n \leq N$. Up to this point everything is independent of how the intervals are chosen. For potentials and initial wave packets that are smooth, it is enough to choose the intervals sufficiently small so that the interaction and initial free wave packet are approximately constant on each interval, I_{mn} . Then the contribution from the potential can be factored out of the integral over the interval, and be replaced by evaluating the potential at any point $y_{mn} \in I_{mn}$ in the interval. In the calculations exhibited in section 6, y_{mn} is taken to be the midpoint of the interval I_{mn} . Because of this, the potential no longer explicitly appears in the integrand, opening up the possibility to treat a large class of potentials. In the limit of small intervals this becomes exact. Thus, the replacement

$$e^{-i \sum_{n=1}^N V(x_n)\Delta t} \langle x_N | \psi_{i0}(-t) \rangle \rightarrow e^{-i \sum_{n=1}^N V(y_{mn})\Delta t} \langle y_{mN} | \psi_{i0}(-t) \rangle. \quad (33)$$

in the integrand of equation (32) is expected to be a good approximation on the cylinder set $I_{m_0} \times I_{m_1} \times \dots \times I_{m_N}$.

Formally the Henstock theory of integration restricts the choice of intervals, evaluation points and time slices needed for convergence. However, for smooth short-ranged potentials and wave packets, the Henstock integrals reduce to ordinary Riemann integrals. Motivated by this, it is assumed that convergence can be achieved using uniformly spaced time slices and intervals of fixed size. Numerical convergence provides an indication of the validity of this assumption.

The replacement (33) leads to the following approximate expression

$$\langle x_0 | e^{-iHs} | \psi_{i0}(-t) \rangle \approx \lim_{N \rightarrow \infty} \lim_{I_{mn} \rightarrow 0} \left(\frac{\mu}{2\pi i \Delta t} \right)^{N/2} \sum_{m_1 \dots m_N} \prod_{n=1}^N \left(\int_{I_{m_n}} dx_n e^{i \frac{\mu}{2\Delta t} (x_{n-1} - x_n)^2} e^{-iV(y_{mn})\Delta t} \psi_{i0}(y_{mN}, -t) \right). \quad (34)$$

The integrals,

$$P(x_0, I_{m_1} \dots I_{m_N}) := \left(\frac{\mu}{2\pi i \Delta t} \right)^{N/2} \prod_{n=1}^N \int_{I_{m_n}} dx_n e^{i \frac{\mu}{2\Delta t} (x_{n-1} - x_n)^2}, \quad (35)$$

are interpreted as complex probabilities to arrive at x_0 by passing through the sequence of intervals $I_{m_N} \dots I_{m_1}$. The probability interpretation follows because the sum of these quantities over all intervals is 1, independent of x_0 :

$$\sum_{m_1 \dots m_N} P(x_0, I_{m_1}, \dots, I_{m_N}) = 1. \quad (36)$$

This is because, using a simple change of variables, the sum can be transformed to the product of N Gaussian-Fresnel integrals that are normalized to unity.

Specifically, $P(x_0, I_{m_1}, \dots, I_{m_N})$ is interpreted as the ‘‘complex probability’’ for a path to pass through I_{m_N} at time t_N , $I_{m_{N-1}}$ at time t_{N-1} , \dots , I_{m_1} at time t_{m_1} , and end up at x_0 at time t . The set of continuous paths that pass through I_{m_N} at time t_N , \dots , I_{m_1} at time t_1 define a cylinder set of continuous paths. The right most (initial) interval only gets contributions from the sample points y_{mN} that are in the support of the initial wave packet. Equation (36) is consistent with the requirement that every continuous path goes through one and only one cylinder set with complex probability 1.

In [11] Nelson defines a path integral by analytically continuing the mass in the kinetic energy term. His probability is related to the analytic continuation in the mass of Muldowney’s complex probability.

In this notation the ‘‘path integral’’ becomes

$$\langle x_0 | e^{-iHt} | \psi_{i0}(-t) \rangle = \lim_{N \rightarrow \infty} \lim_{Vol(I_{mn}) \rightarrow 0} \sum_{m_1 \dots m_N} P(x_0, I_{m_1}, \dots, I_{m_N}) e^{-i \sum_{n=1}^N V(y_{mn})\Delta t} \langle y_{mN} | \psi_{i0}(-t) \rangle. \quad (37)$$

For the half-infinite intervals, I_{0n} and I_{Mn} the upper and lower boundaries increase (resp. decrease) in the limit. Equation (37) is like a Riemann integral with a complex measure, except it is interpreted as the expectation of the random variable $e^{-i\sum_{n=1}^N V(y_{mn})\Delta t} \langle y_{mN} | \psi_{i0}(-t) \rangle$ with respect to the complex probability distribution $P(x_0, I_{m1}, \dots, I_{mN})$. Nathanson and Jørgensen show that the complex probability $P(x_0, I_{m1} \dots I_{mN})$ is concentrated on continuous paths and (37) converges to a global solution of the Schrödinger equation in the limit of finer partitions and more time slices.

This reformulation of Feynman's original path integral provides a justification to represent time evolution in quantum mechanics as an average over paths with complex probabilities. Scattering wave functions are expectation values of the potential functional $e^{-i\int V(\gamma(t))dt}$. Transition matrix elements require an additional multiplication by the potential followed by the Fourier transform of the resulting quantity. For the case of equally spaced sample points this becomes

$$\int \langle p_f | x \rangle V(x) dx \sum_{m_0, m_1 \dots m_N} P(x, I_{m1}, \dots, I_{mN}) e^{-i\sum_{n=1}^N V(y_{mn})\Delta t} \langle y_{mN} | \psi_{i0}(-t) \rangle \approx \frac{1}{\sqrt{2\pi}} \sum_{m_0, m_1, \dots, m_N} e^{-ip_f y_{m0}} \delta y V(y_{m0}) P(y_{m0}, I_{m1} \dots I_{mN}) e^{-i\sum_{n=1}^N V(y_{mn})\Delta t} \langle y_{mN} | \psi_{i0}(-t) \rangle \quad (38)$$

where δy is the width of the I_{mN} interval, and the sum is over the final sample points and the finite intervals, $I_{1N} \dots I_{M-1, N}$.

V. FACTORIZATION

The input to the MNJ formulation of the path integral are the complex probabilities that a path will be in a particular cylinder set of paths. Even if the probabilities $P(x_0, I_{m1}, \dots, I_{mN})$ could be computed analytically, there are $(M+1)^N$ cylinder sets in the limit that M and N become infinite. Summing over all of these configurations is not computationally feasible.

On the other hand, for the case of a single time step, the same approximations that were made for multiple time steps lead to the following

$$\langle x_{N-1} | e^{-iH\Delta t} | \psi_{i0}(-t) \rangle \approx \sum_m P(x_{N-1}, I_{mN}) e^{-iV(y_{mN})\Delta t} \langle y_{mN} | \psi_{i0}(-t) \rangle. \quad (39)$$

This approximates the transformed wave function after one time step. The factorization follows if this wave function is used as the initial state in the transformation to the next time step

$$\langle x_{N-2} | e^{-iH2\Delta t} | \psi_{i0}(-t) \rangle \approx \sum_{m_{N-1}} P(x_{N-2}, I_{m(N-1)}) e^{-iV(y_{m(N-1)})\Delta t} \langle y_{m(N-1)} | e^{-iH\Delta t} | \psi_{i0}(-t) \rangle \approx \sum_{m(N-1), mN} P(x_{N-2}, I_{m(N-1)}) e^{-iV(y_{m(N-1)})\Delta t} P(y_{m(N-1)}, I_{mN}) e^{-iV(y_{mN})\Delta t} \langle y_{mN} | \psi_{i0}(-t) \rangle. \quad (40)$$

Repeating this for all N time steps gives the following approximation

$$\langle x_0 | e^{-iHt} | \psi_{i0}(-t) \rangle \approx \sum P(x_0, I_{m1}) e^{-iV(y_{m1})\Delta t} \prod_{n=2}^N P(y_{m(n-1)}, I_{nm}) e^{-iV(y_{mn})\Delta t} \langle y_{mN} | \psi_{i0}(-t) \rangle \quad (41)$$

where the sum is over the cylinder sets. The factorization leads to the following approximation of the complex probability on the cylinder set $\{I_{m1}, \dots, I_{mN}\}$:

$$P(x_0, I_{m1}, \dots, I_{mN}) \approx P(x_0, I_{m1}) \prod_{n=2}^N P(y_{m(n-1)}, I_{nm}) \quad (42)$$

With this approximation (11) becomes

$$\langle x_0 | V | e^{-iHt} | \psi_{i0}(-t) \rangle \approx$$

$$\sum_{m1 \dots mN} V(x_0)P(x_0, I_{m1})e^{-iV(y_{m1})\Delta t} \prod_{n=2}^N P(y_{m(n-1)}, I_{nm})e^{-iV(y_{mn})\Delta t} \langle y_{mN} | \psi_{i0}(-t) \rangle. \quad (43)$$

This representation has a significant advantage over (37) because the matrix elements

$$K_{m,k} = P(y_m, I_k)e^{-iV(y_k)\Delta t} \quad (44)$$

where

$$P(y_m, I_k) = \left(\frac{\mu}{2\pi i \Delta t}\right)^{1/2} \int_{x_k}^{x_{k+1}} dx e^{i\frac{\mu}{2\Delta t}(y_m - x)^2} = \sqrt{\frac{1}{i\pi}} \int_{\sqrt{\frac{\mu}{2\Delta t}}(x_k - y_m)}^{\sqrt{\frac{\mu}{2\Delta t}}(x_{k+1} - y_m)} e^{i\beta^2} d\beta \quad (45)$$

can be computed analytically, and powers of this matrix can be computed efficiently. The integrals in (45) for finite intervals are Fresnel integrals of the form

$$I[a, b] = \int_a^b e^{ix^2} dx = \sqrt{\frac{\pi}{2}}(C_c(b) - C_c(a)) + i\sqrt{\frac{\pi}{2}}(S_c(b) - S_c(a)). \quad (46)$$

where

$$C_c(x) = \sqrt{\frac{2}{\pi}} \int_0^x \cos(t^2) dt \quad S_c(x) = \sqrt{\frac{2}{\pi}} \int_0^x \sin(t^2) dt. \quad (47)$$

Note that these definitions differ from the definitions of Fresnel integrals given in [12] Abramowitz and Stegun. They are related by

$$C_c(\sqrt{\frac{\pi}{2}}x) = C_{AS}(x) \quad S_c(\sqrt{\frac{\pi}{2}}x) = S_{AS}(x). \quad (48)$$

For the semi-infinite interval with $a = -\infty$

$$I[-\infty, b] = \int_{-\infty}^b e^{ix^2} dx = \frac{1}{2} \int_{-\infty}^{\infty} e^{ix^2} dx - \int_b^{\infty} e^{ix^2} dx = \sqrt{\frac{\pi}{2}} \left(\frac{1+i}{2} + C_c(b) + iS_c(b) \right). \quad (49)$$

and for $b = \infty$

$$I[a, \infty] = \int_a^{\infty} e^{ix^2} dx = \frac{1}{2} \int_{-\infty}^{\infty} e^{ix^2} dx - \int_{-\infty}^a e^{ix^2} dx = \sqrt{\frac{\pi}{2}} \left(\frac{1+i}{2} - C_c(a) - iS_c(a) \right). \quad (50)$$

Using these formulas leads to the following expressions for the one-step matrix K_{mk} when I_k is a finite interval:

$$\begin{aligned} K_{mk} &= P(y_m, I_k)e^{-iV(y_k)\Delta t} = \\ &\frac{1}{2} \left((C_c(\sqrt{\frac{\mu}{2\Delta t}}(x_{k+1} - y_m)) - C_c(\sqrt{\frac{m}{2\Delta t}}(x_k - y_m)) + S_c(\sqrt{\frac{\mu}{2\Delta t}}(x_{k+1} - y_m)) - S_c(\sqrt{\frac{m}{2\Delta t}}(x_k - y_m))) \right. \\ &\left. + i(S_c(\sqrt{\frac{\mu}{2\Delta t}}(x_{k+1} - y_m)) - S_c(\sqrt{\frac{m}{2\Delta t}}(x_k - y_m)) - C_c(\sqrt{\frac{\mu}{2\Delta t}}(x_{k+1} - y_m)) + C_c(\sqrt{\frac{m}{2\Delta t}}(x_k - y_m))) \right) e^{-iV(y_k)\Delta t}. \end{aligned} \quad (51)$$

For $x_k = x_0 = -\infty$:

$$\begin{aligned} K_{mk} &= P(y_m, I_{k0})e^{-iV(y_k)\Delta t} = \\ &\frac{1}{2} \left(1 + (C_c(\sqrt{\frac{\mu}{2\Delta t}}(x_1 - y_m)) + S_c(\sqrt{\frac{\mu}{2\Delta t}}(x_1 - y_m))) + i(S_c(\sqrt{\frac{\mu}{2\Delta t}}(x_1 - y_m)) - C_c(\sqrt{\frac{\mu}{2\Delta t}}(x_1 - y_m))) \right) e^{-iV(y_0)\Delta t} \end{aligned} \quad (52)$$

and for $x_{k+1} = x_{M+1\infty}$:

$$K_{mM} = P(y_m, I_M)e^{-iV(y_M)\Delta t} = \frac{1}{2} \left(1 - (S_c(\sqrt{\frac{m}{2\Delta t}}(x_M - y_m)) + C_c(\sqrt{\frac{m}{2\Delta t}}(x_M - y_m))) - i(S_c(\sqrt{\frac{m}{2\Delta t}}(x_M - y_m)) - C_c(\sqrt{\frac{m}{2\Delta t}}(x_M - y_m))) \right) e^{-iV(y_M)\Delta t} \quad (53)$$

Combining these approximations the expression for $\langle \psi_{f0}(0)|V|e^{-iH\Delta t}|\psi_{i0}(-t)\rangle$ is approximately given by

$$\langle x|V|e^{-iHt}|\psi_{i0}(-t)\rangle \approx \sum_{mk} V(x)P(x, I_m)e^{-iV(y_m)t}K_{mk}^{N-1}\langle y_k|\psi_{i0}(-t)\rangle \quad (54)$$

where K_{mn} is the $(M+1) \times (M+1)$ matrix in equations (51-53). This matrix only requires $M+1$ values of the potential. The other elements needed for this computation are the minimal uncertainty wave function at time $-t$ at the same $M+1$ points and the potential.

While the above formulas are for one-dimensional scattering, the generalization to three dimensions is straightforward. The three-dimensional case involves products of these formulas. Transition matrix elements can be extracted from (54) using (12).

VI. COMPUTATIONAL CONSIDERATIONS

To test this method, approximate transition matrix elements are computed for the example of a particle of mass μ scattering from a repulsive Gaussian potential in one dimension.

From a mathematical perspective the complex probability interpretation assumes that all of the integrals are Henstock-Kurzweil integrals. This means that for given prescribed error, there are restrictions on how to choose the intervals and evaluation points. On the half-infinite intervals the potential is approximately zero and the Henstock-Kurzweil integral is a Fresnel integral that can be computed exactly, while for the finite intervals the Henstock-Kurzweil integrals are Riemann integrals, so convergence can be realized using sufficiently fine, uniformly spaced, space and time grids.

In order keep the analysis as simple as possible (1) N time slices are chosen to be equally spaced and (2) the number, $M-1$, and width δx of the finite intervals on each time slice are chosen to be identical.

There are a number of constraints that have to be satisfied in order to get a good approximation. The Trotter product formula gives the exact result in the limit that $(p^2/2\mu)\Delta t$ and $V\Delta t$ vanish. In a computation these terms need to be small. In the first term p is an unbounded operator, but the limit is a strong limit, so most of the momentum will be centered near the mean momentum of the initial free particle state. This can also be controlled if $m\delta x^2/2\Delta t < 1$. This suggests that both of these dimensionless quantities should be less than 1. A second constraint is that the uncertainty in the momentum of the initial state should be less than the momentum. This avoids having slow moving or backward moving parts of the wave packet that will feel the potential for long times. Because of the uncertainty principle, making Δp small makes Δx large - which increases the time that the wave packet feels the potential. Both $P(x, I_m)$ and $e^{iV(x)\Delta t}$ oscillate, so the widths on the intervals on each time slice need to be small enough so these quantities are approximately constant on each interval. These limits can be realized by choosing sufficiently small time steps and sufficiently narrow intervals. The cost is numerical complexity.

Both the range of the potential and spatial width of the initial wave packet determine the active volume that needs to be broken into small intervals. The velocity of the wave packet determines the elapsed time that the initial wave packet interacts with the potential.

The condition that $\frac{\mu(\delta x)^2}{2\Delta t}$ is small requires N/M^2 to be small, where N is the number of time steps and M is the number of intervals per time step. This means that shortening the time step generally requires including more intervals at each time step.

For the test an initial wave packet with the dimensionless parameters used in the calculations are listed in table 1. The particle scatters off of a Gaussian potential of range r_0 and strength $-v_0$,

$$V(x) = -v_0 e^{-(x/r_0)^2}. \quad (55)$$

The values of the potential parameters used in the test calculations are listed in table 2.

The Trotter product formula is justified provided that the time steps satisfy $p^2/2m\Delta t \approx 12.5\Delta t$ and $V\Delta t \approx 5\Delta t$ are small. The minimum total time is $t = m(r_0 + \Delta x)/p = .6$. The calculations require a slightly longer time for convergence, but convergence can be obtained with a surprisingly large Δt . The active volume is the sum of the width

mass	$\mu = 1.0$
initial momentum	$p_i = 5.0$
momentum uncertainty	$\Delta p_i = 0.25$
position uncertainty	$\Delta x = 2.0$
initial velocity	$v_i = p_i/\mu = 5.$

TABLE I: initial wave packet parameters

strength	$v_0 = 5.0$
range	$r_0 = 1.0$

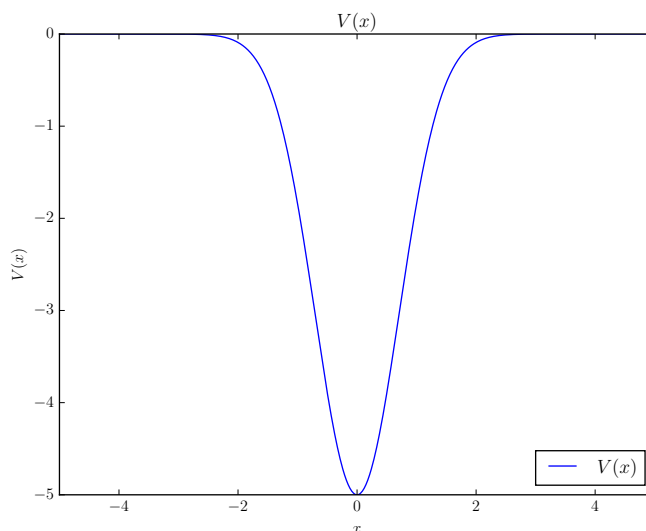
TABLE II: potential parameters

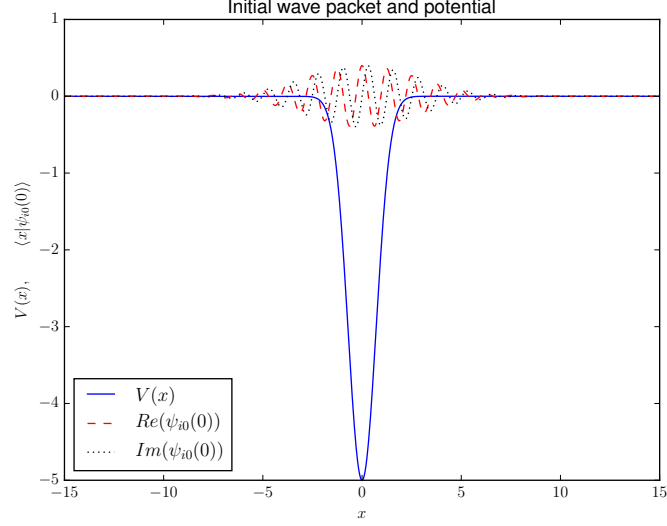
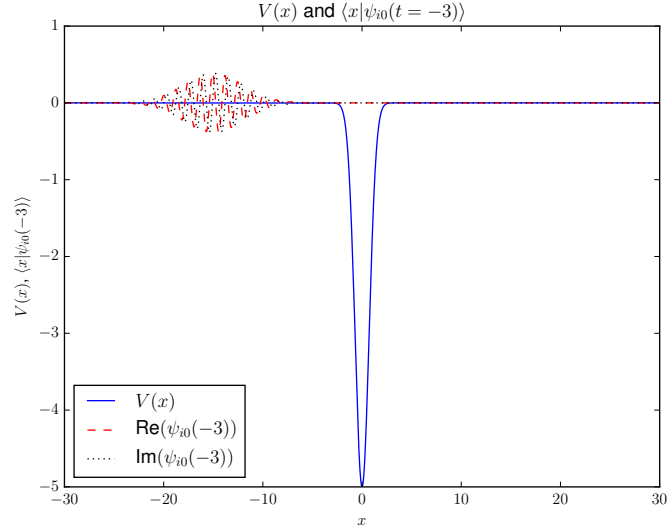
of wave packet plus the range of the potential, which is about 3.0 units. This must be decomposed into small intervals where the potential and wave packet vary slowly.

Figure 1: Shows the potential (55) in configuration space. It gives a more precise measure of the full width of the potential, which is just over about 4.0 units.

Figure 2: Shows the real and imaginary parts of the initial free wave packet $\langle x|\psi_{0i}(0)\rangle$ and plots of the potential on the same graph. What is relevant is the combined width of the initial wave packet and the potential. In this figure the potential is represented by the solid line, the real part of the initial wave packet is represented by the dashed line and the imaginary part of the initial wave packet is represented by the dotted line. This figure can be used to estimate the active volume needed for a calculation. An estimate of the minimum t needed for convergence is the time it takes for the wave packet to no longer feel the effects of the potential. Figure 2 shows that the width initial wave packet is about twice the width of the potential. These graphs suggest that the active volume is actually about 12 units. For a wave packet moving with speed $v = p_i/m = -5$ the wave packet will travel 15 units in a time $t = 3.0$. This should be sufficiently long to move the potential out of the range of the potential if the spreading of the free wave packet is ignored. The effect of the spreading can be included by comparing the free wave packet at time $t = -3$ with the potential. This is illustrated in figure 3 which plots the real and imaginary parts of the initial free wave packet at time $t = -3$ with the potential. As in figure 2 the potential is represented by the solid line, the real part of the initial wave packet is represented by the dashed line and the imaginary part of the initial wave packet is represented by the dotted line. Figure 3 shows that even with the effects of wave-packet spreading, at $t = -3.0$ the wave packet has not reached the range of the potential. This suggests that $t = 3.0$ is a good first guess at the time t sufficient for convergence of $\Omega(-t)|\psi_{0i}(0)\rangle$.

Numerical calculations are possible because of the factorization of the complex probabilities into products of matrix

FIG. 1: $V(x)$

FIG. 2: $V(x), \langle x|\psi_{0i}(0)\rangle$ FIG. 3: $V(x), \langle x|\psi_{0i}(-3)\rangle$

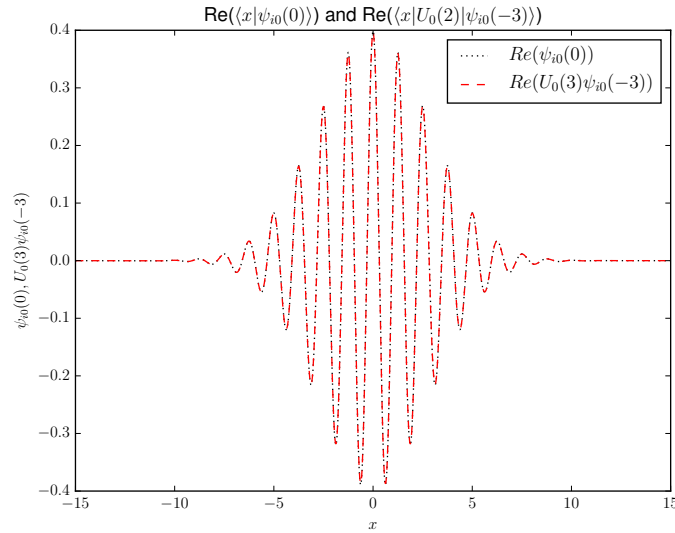
elements of one-step probabilities. Table 3 shows the sum of $M=5000$ one-step complex probabilities computed at different points. The computation shows that these quantities behave like complex probabilities. The real part of the sum of 5000 complex probabilities is always 1 and the imaginary part is always 0, independent of the final x value. The table indicates the stability of the sum of these large numbers of one-step complex probabilities since the cancellation of all of the imaginary terms is accurate to 15-17 significant figures.

The accuracy of the numerical computation of the time evolution of the initial wave packet depends on having sufficiently small δx and Δt . The limiting size depends on the initial wave packet.

Since the time evolution of the free wave packet can be computed analytically, one test of accuracy of the free evolution based on using products of one-step probabilities is to start with the exact initial wave packet at $t = -3$ and transform it back to the initial time, $t = 0$, using multiple applications of the one-step probability matrices to the exact wave packet at $t = -3$. This can then be compared to the exact initial wave packet at $t = 0$. In this test $t = -3$ is chosen because the wave packets should have reached the asymptotic region by then. This test used 30 time steps separated by $\Delta t = .1$ and 5000 spatial steps between -25 and 25 corresponding to a spatial resolution $\delta_x = .01$.

x	$\sum_n \Re(P_n(x))$	$\sum_n \Im(P_n(x))$
-25.005001	p=1.000000e+00	+ i(5.273559e-16)
-20.204041	p=1.000000e+00	+ i(-1.387779e-16)
-15.003001	p=1.000000e+00	+ i(2.775558e-17)
-10.202040	p=1.000000e+00	+ i(2.775558e-16)
-5.001000	p=1.000000e+00	+ i(7.771561e-16)
0.200040	p=1.000000e+00	+ i(3.608225e-16)
5.001000	p=1.000000e+00	+ i(1.665335e-16)
10.202040	p=1.000000e+00	+ i(5.273559e-16)
15.003001	p=1.000000e+00	+ i(8.049117e-16)
20.204041	p=1.000000e+00	+ i(1.137979e-15)
25.005001	p=1.000000e+00	+ i(-2.164935e-15)

TABLE III: sums of complex probabilities

FIG. 4: Real part of $\langle x|\psi_{0i}(0)\rangle$ and $\langle x|U_0(3)|\psi_{0i}(-3)\rangle$

The result of this calculation is shown in figures 4 and 5. These figures compare

$$\psi_{i0}(x, 0) \quad \text{to} \quad \sum P(x, I_{n1})P(y_{n1}, I_{n2}) \cdots P(y_{n19}, I_{n20})\langle y_{n20}|\psi_{0i}(-3)\rangle. \quad (56)$$

Figures 4 and 5 show the real and imaginary parts of the exact $t = 0$ free wave function and the exact $t = -3.0$ free wave function evolved back to $t = 0$ with 30 time slices. These calculations used $\Delta t = .1$ and $\delta x = .01$. In these plots the dashed lines represent the calculated $t = 0$ wave function while the dotted line represents the exact $t = 0$ wave function given in (17).

In these figures both the real and imaginary parts of both wave functions fall on top of each other. This suggests that both the time steps and resolution are sufficiently small to evolve the free wave packet for $t = 3.0$

In these calculations there was no attempt at efficiency; however because of the analytic expressions for the one-step probabilities, the one-step probabilities were computed on the fly in order to avoid storing matrices. The resolution was chosen to be sufficiently fine to represent the initial wave packet.

The next two figures illustrate the effect of the potential on the evolution of the wave function. Figure 6 compares the real part of the scattering wave function $\langle x|\psi_i(0)\rangle = \langle x|\Omega(-3.0)|\psi_{i0}(0)\rangle$ (dotted line) at time $t = 0$ to the initial wave packet $\langle x|\psi_{i0}(t = 0)\rangle$ at $t = 0$. The parameters used for this computation are $\Delta t = .1$, $\delta_x = .01$ and $x \in [-25, 25]$, which are the same parameters used to produce figure 4. The functions are calculated at the midpoint of each finite interval. Figure 7 shows the corresponding plot for the imaginary part of the wave function. Figures 6 and 7 show the change in phase as the interaction is turned on. The dashed lines in both figures represent the initial wave packet, while the dotted lines represent the interacting wave packet.

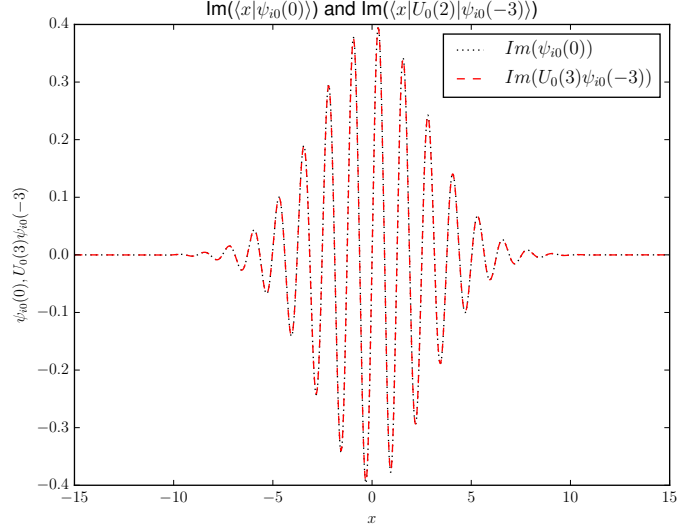


FIG. 5: Imaginary part of $\langle x|\psi_{0i}(0)\rangle$ and $\langle x|U_0(3)|\psi_{0i}(-3)\rangle$

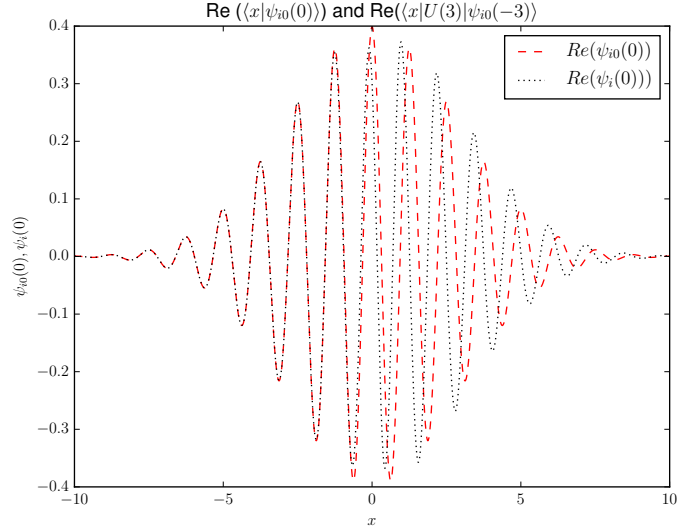


FIG. 6: Real part of $\langle x|\psi_{0i}(-3)\rangle$ and $\langle x|\psi_i(-3)\rangle$

Note that these calculations approximate the incident scattered wave function at the collision time ($t = 0$). This is why the wave functions do not look like separated transmitted and reflected waves. As discussed in section 2, the exact incident wave function at $t = 0$ is sufficient to compute the differential cross section. These figures also show that both the free and interacting $t = 0$ wave functions occupy approximately the same volume, (about 20 units) which shows that using $\Omega(t)$ to calculate the scattering wave function eliminates spreading of the wave function.

With the potential turned on it is important to check that (1) the volume $[-25, 25]$ is sufficiently large, the time step $\Delta t = .1$ is sufficiently small, the resolution $\delta_x = .01$ is sufficiently small, the total time $t = 3.0$ is sufficiently large, and the calculation is stable with respect to changing the sample point y_i in the interval I_i .

Note that all of the calculations assume that the evolved wave functions vanish on the half infinite intervals. This is justified both graphically and because the wave packet remains square integrable.

The Trotter product formula is justified in the small time step limit. The calculations illustrated in figures 6 and 7 used a time step $\Delta_t = .1$. Figures 8 and 9 compare real and imaginary parts of the scattered wave function $\langle x|\psi_i(0)\rangle = \langle x|\Omega(-3.0)|\psi_{i0}(0)\rangle$ using a time step size of $\Delta_t = .1$ (dashed curve) with corresponding calculations using

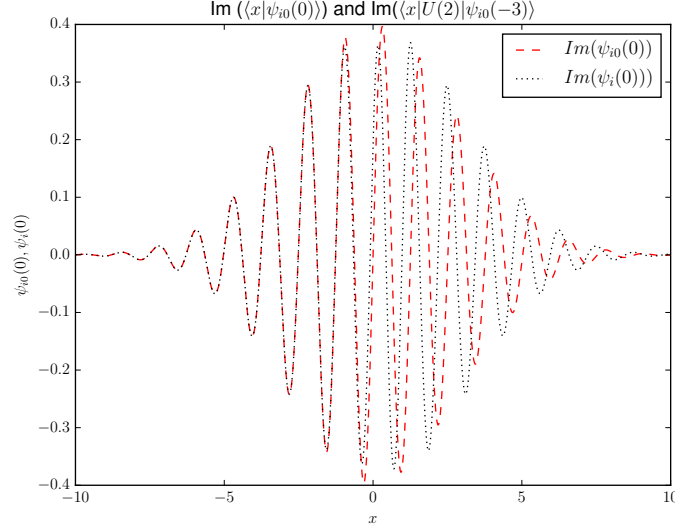


FIG. 7: Imaginary part of $\langle x|\psi_{0i}(-3)\rangle$ and $\langle x|\psi_i(-3)\rangle$

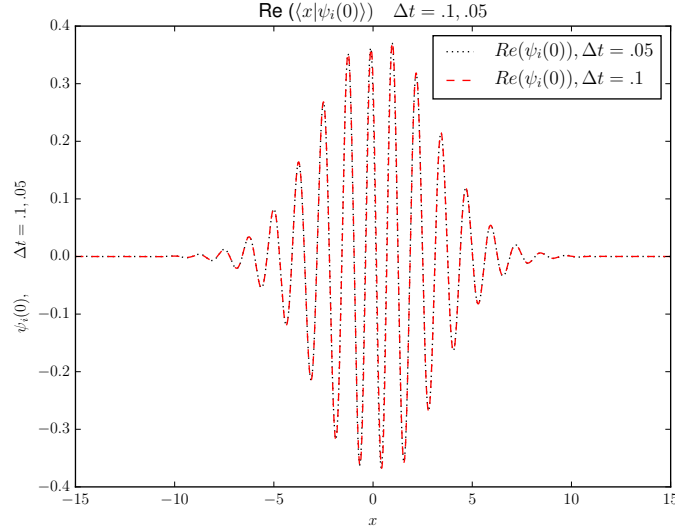
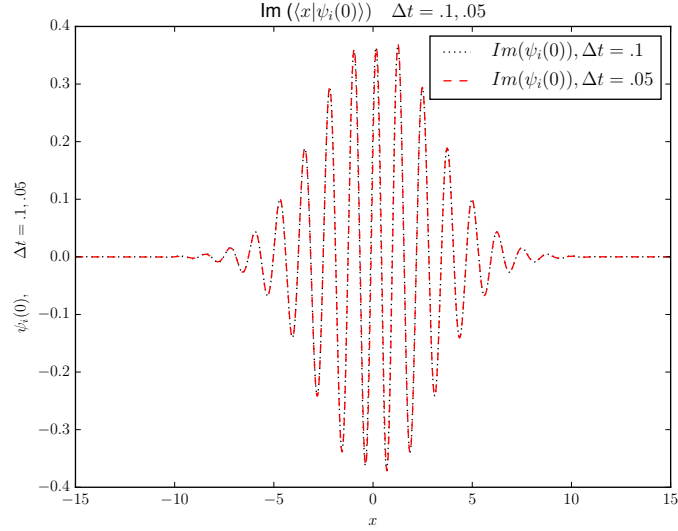
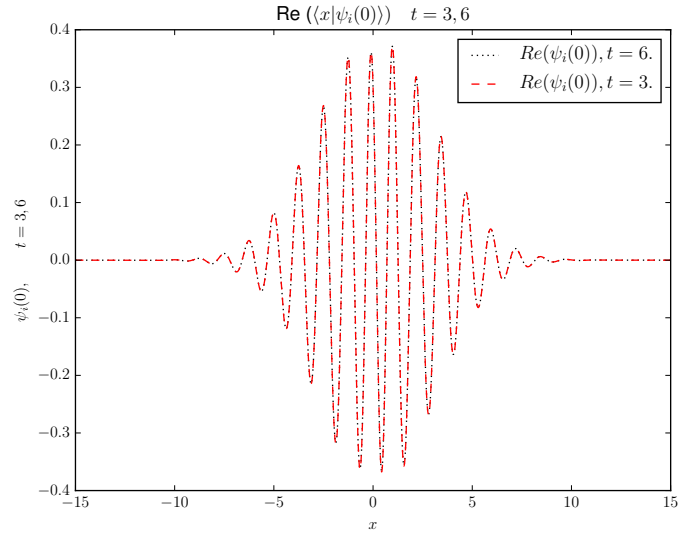


FIG. 8: $\Delta t = .1, .05$

a time step of half the size, $\Delta t = .05$ (dotted curve). The plots of the real and imaginary parts of the scattered $t = 0$ wave functions for $\Delta t = .1$ and $\Delta t = .05$ fall on top of each other. This indicates that the time resolution Δt is sufficiently fine for this calculation

The initial choice of the approximating $\Omega_- := \lim_{t \rightarrow -\infty} \Omega(t)$ by $\Omega(-3)$ was determined by examining the range of the potential and width and speed of the wave packet. Figure 10 and 11 show the effect of increasing the time from $t = 3.0$ to $t = 6.0$, keeping the size of the time step $\Delta t = .1$ constant, on the real and imaginary parts of the calculated scattering wave function. The plots of the wave functions for $t = -3.0$ (dashed curve) and $t = -6.0$ (dotted curve) fall on top of each other. This suggests that $t = 3.0$ is sufficient for convergence.

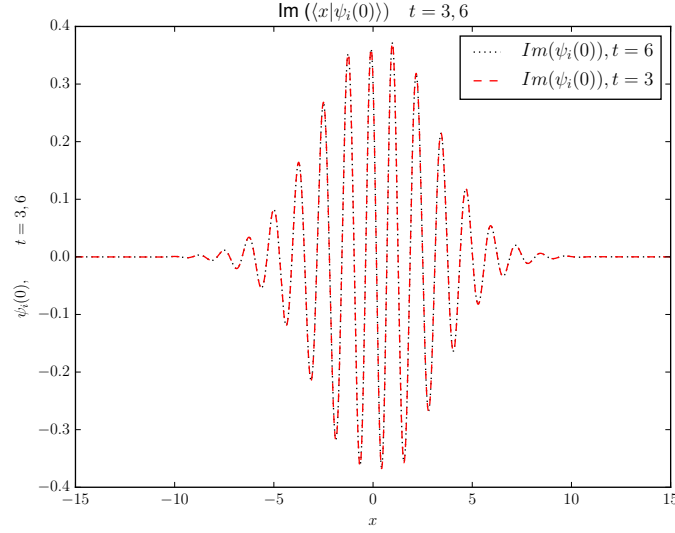
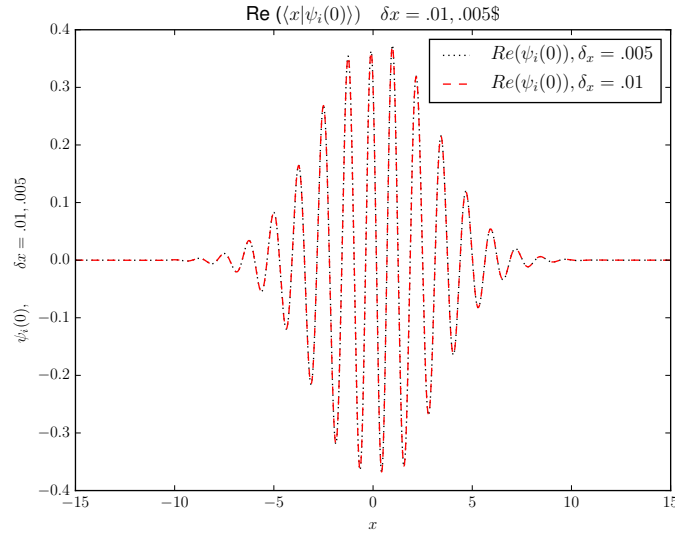
Due to the oscillating nature of the wave function, the spatial resolution of the intervals that define the cylinder sets should be sufficiently small that the wave function is effectively constant on them. Figures 12 and 13 show the effect of increasing the spatial resolution from 5000 intervals ($\delta_x = .01$, dashed curves) to 10000 intervals ($\delta_x = .005$, dotted curves) on the real and imaginary parts of the scattering wave function. In these calculations $\Delta t = .1$, $t = 3.0$ and the interval is $[-25, 25]$. Again the curves for the real and imaginary part of the wave function fall on top of each

FIG. 9: $\Delta t = .1, .05$ FIG. 10: $t = 3.0, 6.0$

other. This indicates that for this problem a spatial resolution $\delta_x = .01$ (5000 intervals) is sufficient for convergence.

While the previous plots suggest that wave functions vanish outside of the volume $[-25, 25]$, it is still important to check that the results are stable with respect to increasing the active volume of the calculation. Figures 14 and 15 compare calculations of the real and imaginary parts of the wave function where the volume is changed from $[-25, 25]$ (dotted curves) to $[-50, 50]$ (dashed curves) keeping $\delta_x = .01$, $\Delta t = .1$, and $t = 3$. Again, the calculations indicate the volume $[-25, 25]$ is sufficient for convergence.

The size of the spatial intervals, δx , should be sufficiently small that the potential and initial wave free wave packet are approximately constant on the intervals. Figures 16 and 17 compare calculations where the potential is evaluated at the center or left endpoint of each interval for $\delta x = .01$ Figure 16 shows the real part of the wave function, where the sample points are at the left (dash-dot line) and the center (dashed line) of the interval. Figure 17 shows the imaginary part. This tests whether the potential is locally constant on each interval. These graphs show a small shift in the overall phase of the wave function. Figures 18 and 19 repeat the calculations shown in Figures 16 and 17 by increasing the resolution by a factor of 2. These figures show a corresponding reduction in the difference between the

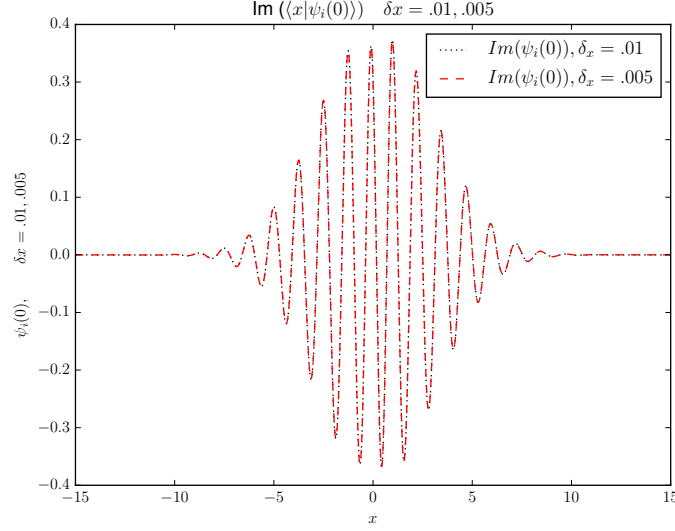
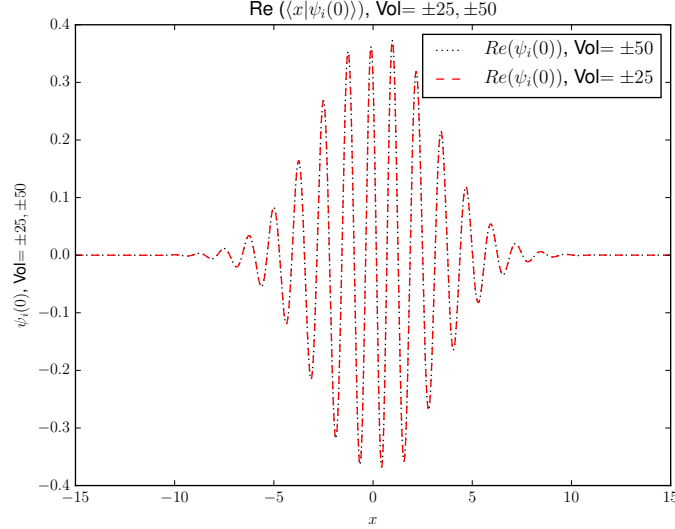
FIG. 11: $t = 3.0, 6.0$ FIG. 12: $\delta x = .01, .005$

two curves.

The goal of this work is to determine if these scattering wave functions can be used to calculate sharp-momentum transition matrix elements. Because the limits in the Trotter product formula the initial momentum was replaced by a narrow wave packet. To test the effect of the smearing, the sharp-momentum Born approximation is compared to the Born approximation where the initial sharp momentum state is replaced by a Gaussian delta function of width .25, which was used in the calculations above.

This comparison is illustrated in figure 20. The solid curve shows the Gaussian approximation to the delta function with width $\Delta p = .25$. The dotted curve shows the potential with initial momentum $p = 5$, as a function of the final momentum. The dashed curve shows the same potential with the initial momentum replaced by the Gaussian delta function state centered at $p = 5$ as a function of the final momentum. The figure shows a small decrease in the matrix elements due to the smearing near the on-shell value.

As another test of the numerical convergence, the smeared Born approximation $\langle p | V | \Psi_{i0}(0) \rangle$ is compared to $\langle p | V \Omega_0(V = 0, t = 3) | \Psi_{i0}(-3) \rangle$, where the *potential is turned off* to compute $\Omega_0(3)$. In this calculation $\delta x = .01$

FIG. 13: $\delta_x = .01, .015$ FIG. 14: $\Re, Vol = \pm 25, \pm 50$

and $\Delta t = .1$. This comparison is shown in figure 21. The imaginary part of $\langle p | V \Omega_0(V = 0, t = 3) | \Psi_{i0}(-3) \rangle$, shown in the solid line should vanish, while the real parts of $\langle p | V | \Psi_{i0}(0) \rangle$ (dotted line) and $\langle p | V \Omega_0(V = 0, t = 3) | \Psi_{i0}(-3) \rangle$ (dashed line), should agree. The figure shows that the calculation accurately approximates the smeared Born approximation.

The approximate calculations give $V(x) \langle x | \Omega(t) | \psi_{i0}(-t) \rangle$. The sharp-momentum transition matrix elements can be computed using a direct Fourier transform (12) or by integrating against Gaussian delta function with the desired final momentum (13). These two methods of calculation are compared in figures 22 and 23. In these calculations the Δp of the final Gaussian is .25, which is the same value used in the initial Gaussian. The dashed curves show the real and imaginary parts of the smeared transition matrix elements computed using a direct numerical Fourier transform (dash dot curves) compared to the curves which show the corresponding quantities that replace the final momentum by a Gaussian approximation to a delta function (solid curves). For these calculations the time step was taken to be $\Delta t = .025$, and $\Delta x = .003$ which is smaller than the time step used in the calculations shown in figures 4-7 and 10-19. This is because the T -matrix calculations, which involve Fourier transforms or integration against oscillating wave

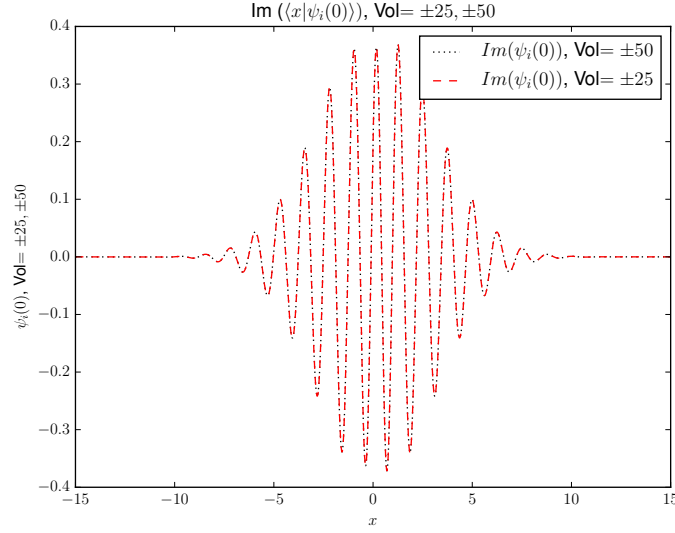
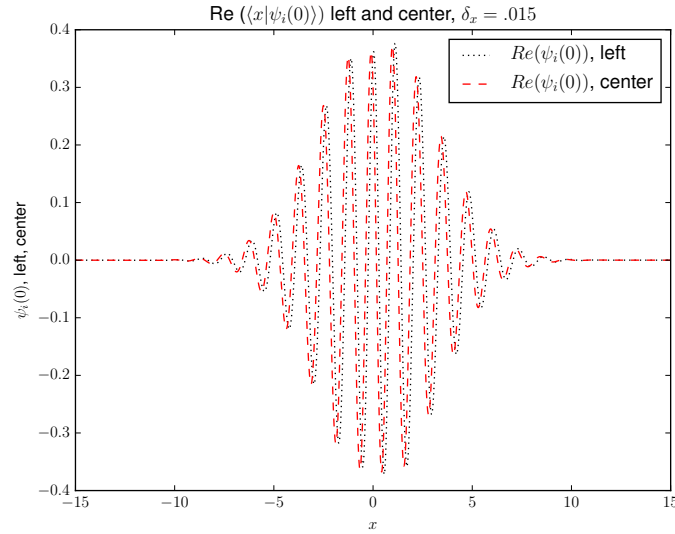
FIG. 15: $\Im, Vol = \pm 25, \pm 50$ 

FIG. 16: Re left vs center

packets, are more sensitive to the accuracy of the scattering wave functions. These figures show that both methods give results within a few percent of each other.

Figures 24 and 25 compare the smeared transition matrix elements (using the direct Fourier transform method - dash-dot curves) to sharp momentum transition matrix elements computed by numerically solving the Lippmann-Schwinger equation (dashed curves) using the method in [13]. The Lippmann-Schwinger calculations are represented by the dashed curve while the path integral calculations are represented by the dotted curve. As with the other calculation errors are a few percent at the on shell point. The comparison is between a sharp-momentum matrix element and a matrix element where the initial state is smeared with a narrow wave packet, so there will be some residual difference due to the smearing. The curves in fig 20. suggest that this effect is a few percent. All of the errors can be reduced at the expense of a larger calculation.

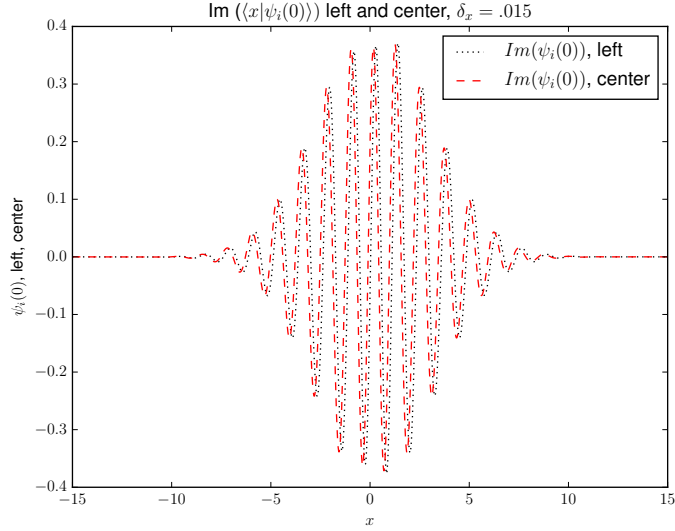


FIG. 17: Im left vs center

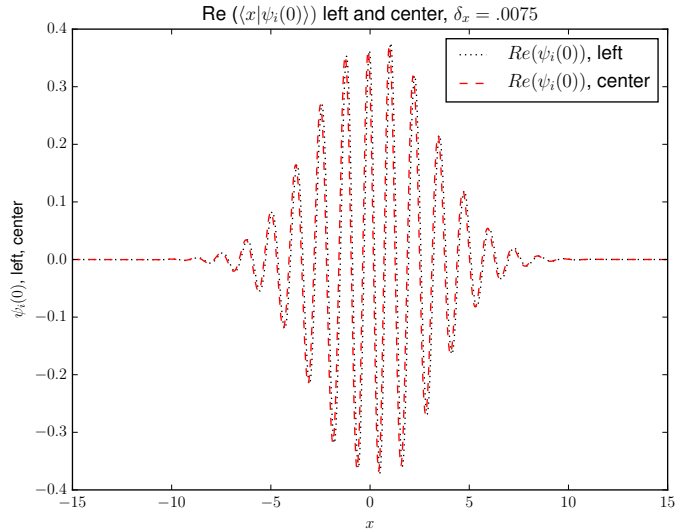


FIG. 18: Re left vs center

VII. SUMMARY AND CONCLUSIONS

This work demonstrated the feasibility of performing scattering calculations using real-time path integrals. The calculations were based on a reinterpretation of the path integral as the expectation value of a potential functional with respect to a complex probability distribution on a space of paths.

The space of paths was constructed by dividing the total time into a large number of small time slices. At each time slice space was divided up into a large number of small windows, including two semi-infinite windows. The space of continuous paths can then be decomposed into disjoint equivalence classes where equivalent paths pass through the same intervals at each time slice.

A complex probability is assigned to each equivalence class. It is constructed by decomposing the propagation of a free quantum mechanical system into a sum of parts associated with each equivalence class. Interactions are introduced by considering the effects of the potential at each window. Mathematically the time evolution of an initial wave packet is represented by an average of a path dependent potential functional on the space of paths with respect

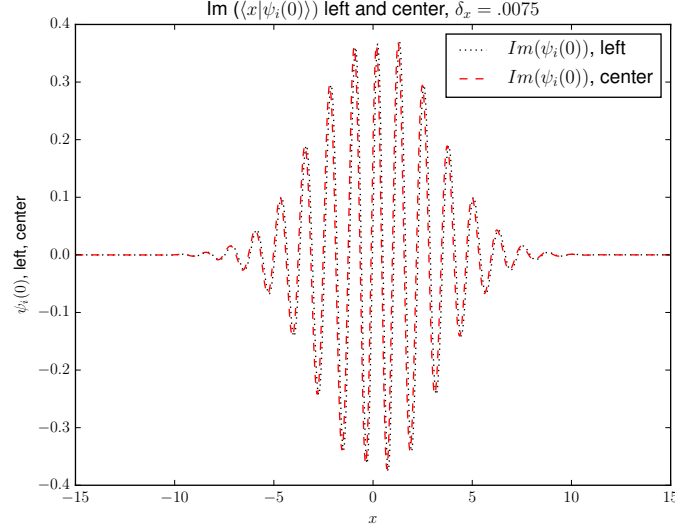


FIG. 19: Im left vs center

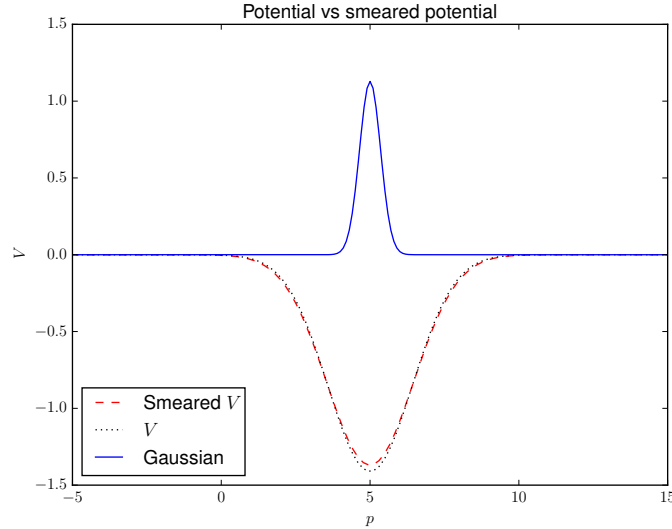


FIG. 20: Born approximation vs smeared Born approximation

to the complex probability distribution.

For the convergence of the calculations the equivalence class of paths must be sufficiently fine that the potential functional has approximately the same value for all paths in the same equivalence class. In addition, the time steps must be sufficiently small for the Trotter product formula to converge.

The difficulty is the large number of equivalence classes. Each equivalence class can be represented as the intersection of N one step classes for each time step. This can be used to make an approximate factorization of the N -time step complex probability as a product of N one-time-step probabilities. This approximation replaces the sum over the large number of equivalence classes by computing powers of a large matrix, which is the basis of the illustrated calculations. In this representation the contribution of each equivalence class is approximated by a particular sequence of products of matrix elements. For example, if M_{mn} represents the one step probability matrix, the product of numbers

$$M_{n_0 n_1} M_{n_1 n_2} \cdots M_{n_{19} n_{20}} \quad (57)$$

is approximately the complex probability for passing through the sequence of windows $I_{n_{20}}$ at time t_1 , $I_{n_{19}}$ at time t_2, \dots . This factorization represents a tremendous increase in efficiency - by using matrix algebra to treat a large

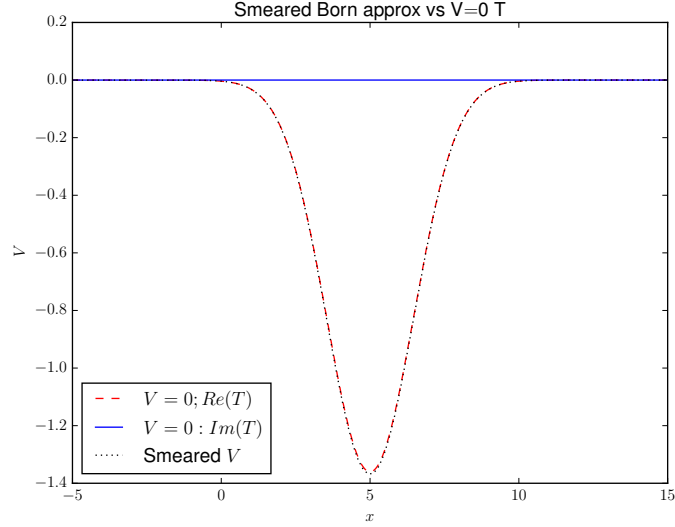


FIG. 21: Exact smeared Born approximation vs $V=0$ wave function Born approximation

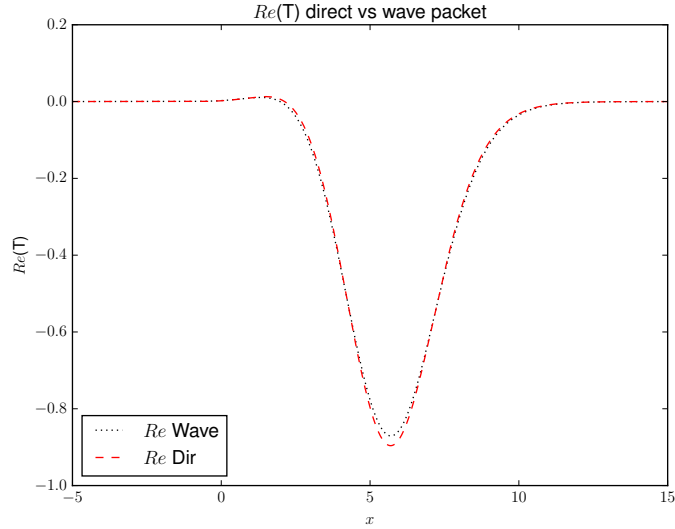


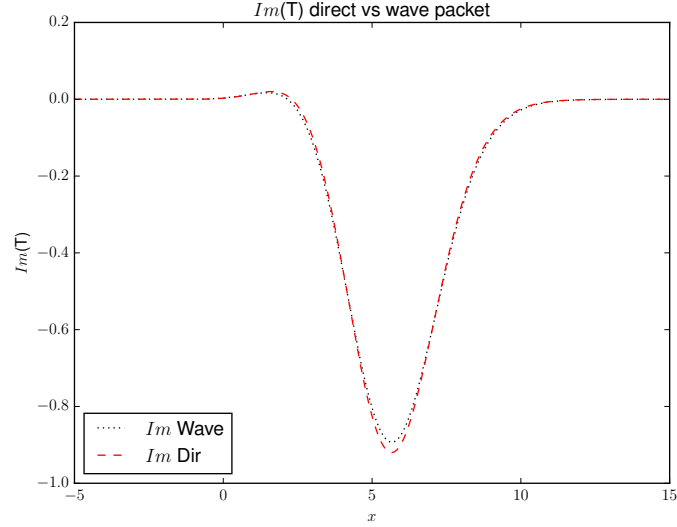
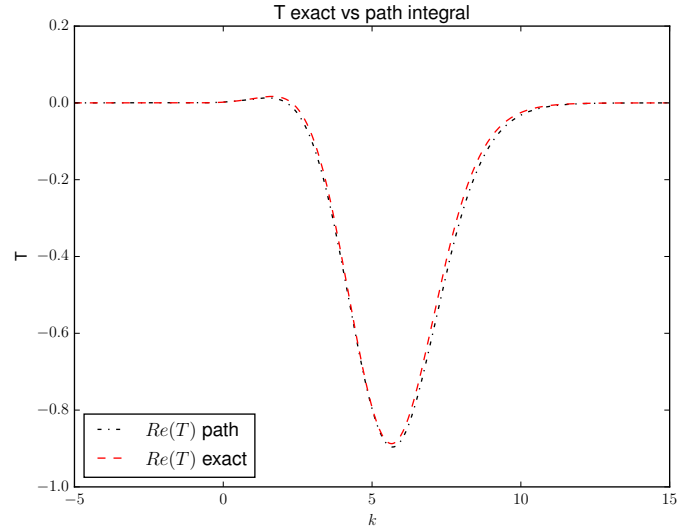
FIG. 22: $\text{Real}(T)$ - Fourier transform vs wave packet

number of equivalence classes of paths in parallel. This looks like replacing the path integral by successive applications of a transfer matrix to an initial state, except in this case it is possible to identify and extract the contribution of each equivalence class of paths to the free-particle time-evolution operator.

The scattering calculations were performed by approximating Møller wave operators [14] applied to normalizable wave packets. This has the advantage of removing wave packet spreading effects from the scattering calculations.

The calculations presented in this paper formally involve applying the 30^{th} power of a 5000×5000 matrix to a fixed vector (for the transition matrix element calculations the 100^{th} power of a 10000×10000 matrix). This corresponds to averaging over 5000^{30} (resp $(10000)^{100}$) equivalence classes of paths. Because the one-step probabilities could be computed analytically, accurately and efficiently, matrix elements could be computed on the fly, which means that the computer storage required for these calculations amounted to storing few complex vectors of length $5000(10000)$. Most of the calculations took a few minutes on a desktop personal computer. One of the surprising aspects of these calculations is the stability of the sums over the complex probabilities.

The one positive is that in all cases of interest the relevant volume is finite; it is limited by the range of the

FIG. 23: $\text{Re}(T)$ - Fourier transform vs wave packetFIG. 24: $\text{Re}(T)$ exact vs path integral

interactions and size of the wave packets.

The calculations presented were performed in minutes on a desktop computer. No attempt was made to be efficient. All intervals and time steps were taken to be the same size. This is the analog of computing a Riemann integral with equally spaced intervals. There is a great deal of freedom both in how to choose intervals and time slices that was not exploited. No attempt was made to compute powers of the product of the one step probability matrix with the potential matrix. The presented calculations simply applied the same matrix N times to the initial vector. The application of the one-step probability matrix to a localized vector could be made more efficient by discarding small components of the resulting vector, reducing the size of the vector that must be stored for each time step. None of these potential efficiencies were utilized.

Beyond the numerical considerations, this framework is appealing in that the input is a potential functional $F[\gamma]$; this picture is retained both exactly and in approximation. This is in contrast to the usual path integral where the relevant weight functional formally looks like an action, but the terms that represent the time derivatives have no legitimate interpretation as derivatives in the Trotter product formula. In the MNJ formulation, these terms do not

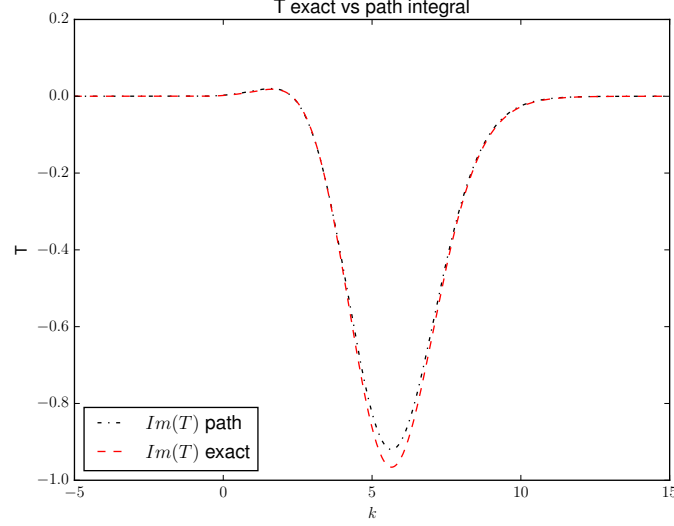


FIG. 25: Im(T) exact vs. path integral

appear explicitly; they are contained in the expression for the one-step probabilities

While the calculations in this paper are motivated by the complex probability interpretation, the computational strategy can be understood directly from the Feynman's work. His path integral results in the kernel $K(x, t; x', t')$ of the time evolution operator (see equation (4.2) of [2])

$$\langle x|\psi(t)\rangle = \int K(x, t; x', t') dx' \langle x'|\psi(t')\rangle \quad (58)$$

This can be expressed as the product of propagation over many time steps (see equation (2.33) of [2]) :

$$\langle x|\psi(t)\rangle = \int K(x, t; x_1, t_1) dx_1 K(x_1, t_1; x_2, t_2) dx_2 \cdots K(x_{N-1}, t_{N-1}; x_N, t_N) dx_N \langle x_N|\psi(t_N)\rangle \quad (59)$$

If the time intervals $t_{j+1} - t_j$, are sufficiently small then

$$K(x_{j+1}, t_{j+1}; x_j, t_j) \approx K_0(x_{j+1}, t_{j+1}; x_j, t_j) e^{-iV(x_j)(t_{j+1}-t_j)} \quad (60)$$

where $K_0(x_{j+1}, t_{j+1}; x_j, t_j)$ is the free time-evolution kernel. This is justified by the Trotter product formula. Finally, if the integrals were replaced by numerical quadratures, this would become

$$\begin{aligned} \langle x|\psi(t)\rangle \approx \sum K_0(x, t; x_{1n_1}, t_1) e^{-iV(x_{1n_1})(t-t_1)} \Delta_{x_{1n_1}} K_0(x_{1n_1}, t_1; x_{2n_2}, t_2) e^{-iV(x_{2n_2})(t_1-t_2)} \Delta_{x_{2n_2}} \cdots \times \\ K_0(x_{(N-1)n_{N-1}}, t_{N-1}; x_{Nn_N}, t_N) e^{-iV(x_{Nn_N})(t_{N-1}-t_N)} \Delta_{x_{Nn_N}} \langle x_N|\psi(t_N)\rangle \Delta_{x_{2n_2}}. \end{aligned} \quad (61)$$

The quantity

$$K_0(x_{1n_1}, t_1; x_{2n_2}, t_2) \Delta_{x_{2n_2}} \approx \int_{x_{2n_2}-\Delta_{x_{2n_2}}/2}^{x_{2n_2}+\Delta_{x_{2n_2}}/2} K_0(x_{1n_1}, t_1; x, t_2) dx \quad (62)$$

corresponds to the one-step probability used in this work. If this replacement is made in (61) the result is equivalent to (37). The important features to emphasize are (1) because of the small time steps, the potential can be factored out and evaluated at one of the quadrature points and (2) the free particle kernel is known. It is these two features that make non-trivial calculations possible.

The interesting question is whether this method can be scaled to more particles or fields? Considering the information needed to perform these one-dimensional calculations, it is expected that few-body calculations will be feasible,

however applications to many-body systems or fields do not appear to be feasible in the absence of a significant advance in computational strategy.

Some observations may be relevant in this context. Conceptually, the one-step probability multiplied by the one step-potential functional, $e^{-iV(y_i)\Delta t}$, which is the key to the computational method, is essentially a transfer matrix, which is a unitarized version of using the Hamiltonian to solve the Schrödinger equation for finite time by taking many small time steps. This has a lot in common with evolving a product of smeared field operators with the Heisenberg equations of motion. Also, the one-step complex probability is essentially free propagation over short time, which is also well understood in the field-theory case. The connection with this interpretation of the real-time path integral with time evolution based on a transfer matrix may be valuable to explore in this context.

One of the authors (WP) would like to acknowledge the generous support of the US Department of Energy, Office of Science, grant number DE-SC0016457 who supported this research effort.

-
- [1] R. Feynman, *Reviews of Modern Physics* **2**, 367 (1948).
 - [2] R. Feynman and A. R. Hibbs, *Quantum Mechanics and Path Integrals* (McGraw-Hill, USA, 1965).
 - [3] P. Muldowney, *A Modern Theory of Random Variation* (Wiley, N.J., 2012).
 - [4] E. S. Nathanson and E. Jørgensen, *Palle*, *J. Math. Phys.* **56**, 092102 (2015).
 - [5] E. S. Nathanson, University of Iowa Thesis (2015).
 - [6] R. Henstock, *Theory of Integration* (Butterworths, London, 1963).
 - [7] R. G. Bartle, *A modern theory of integration*, vol. 32 (American Mathematical Society, Providence, RI, 2001).
 - [8] T. Gill and W. Zachary, *Real Analysis Exchange* **34**, 1 (2008).
 - [9] M. Reed and B. Simon, *Methods of Modern Mathematical Physics*, vol. I (Academic Press, San Diego, 1980).
 - [10] B. A. Lippmann and J. Schwinger, *Physical Review* **79**, 409 eq 1.63 (1950).
 - [11] E. Nelson, *Journal of Mathematical Physics* **5**, 332 (1964).
 - [12] M. Abramowitz and I. Stegun, *Handbook of Mathematical Functions*, vol. 55 (National Bureau of Standards, Washington DC., 1964).
 - [13] O. A. Rubtsova, V. N. Pomerantsev, and V. I. Kukulkin, *Physical Review C* **79**, 064602 (2009).
 - [14] C. Møller, *Det. Kgl. Danske Videnskaberbernes Selskab, Matematisk-Fysiske Meddelelser* **23(1)** (1945).